RSC Advances

PAPER

View Article Online
View Journal | View Issue

Cite this: *RSC Adv.*, 2017, **7**, 31221

Development of Mg–Al–La tri-metal mixed oxide entrapped in alginate for removal of fluoride from wastewater

Aihe Wang,[ab] Kanggen Zhou,*[a] Xing Liu,[a] Fang Liu[a] and Quanzhou Chen[a]

Received 2nd March 2017
Accepted 7th June 2017

DOI: 10.1039/c7ra02566a

rsc.li/rsc-advances

New biopolymer beads, composed of a Mg–Al–La tri-metal oxide (MAL) and alginate (SA), were synthesized, characterized and tested for their fluoride removal efficiency from wastewater. The morphology and properties of the beads were characterized by Fourier transform infrared spectroscopy (FTIR), X-ray photoelectron spectroscopy (XPS) and scanning electron microscopy (SEM). Batch sorption studies were carried out to investigate the adsorption capacity of fluoride on SA-CMAL. The equilibrium sorption data were analyzed using the adsorption isotherm models of Langmuir and Freundlich. To explore the adsorption mechanism, thermodynamic parameters including ΔH^0, ΔS^0 and ΔG^0 were calculated from the results of adsorption thermodynamics. The maximum adsorption capacity of fluoride adsorption on SA-CMAL was 30.96 mg g^{-1} at 303 K. Compared with the Langmuir model, the Freundlich isotherm model better fitted the equilibrium data. In addition, the adsorption process was best fitted with pseudo-second-order kinetics. The value of the thermodynamic parameter ΔH^0 indicated an exothermic adsorption process. A negative value of ΔG^0 shows the feasibility and spontaneity of material–anion interaction. The detrimental effect of co-existing anions increased in the order $SO_4^{2-} < NO_3^- < CO_3^{2-} < PO_4^{2-}$.

1. Introduction

Fluoride is a natural element which is released into the environment by natural processes and anthropogenic activities (*e.g.*, production of phosphate fertilizers, aluminum smelting, and chemical manufacturing).[1] Fluoride is essential for the prevention of dental cavities, but its high level in the body can lead to dental and skeletal fluorosis, which makes bones brittle and vulnerable to fracture. The maximum permissible limit of fluoride in a secondary maximum contaminant level is set at 2.0 mg L^{-1} by the U.S. Environmental Protection Agency.[2] Therefore, in recent years tremendous efforts have been made for mitigation of excess fluoride in wastewater.

Various technologies have been applied for the purification of fluoride contaminated water, such as coagulation–precipitation,[3] induced crystallization,[4] ion exchange, membrane filtration,[5] electro dialysis[6,7] and adsorption.[8] Among them, adsorption is the most widely used and preferred method owing to its simplicity of operation and the availability of a wide range of adsorbents. In recent years, considerable attention has been focused on the study of fluoride removal using composite materials. For example, cuttlefish bones,[9] magnesia-loaded fly ash,[10] Zr(IV) loaded dried orange juice residue,[11] hydrous Ce(IV) + Zr(IV) mixed oxide,[12] and Fe–Ca–Zr,[13] have shown very promising results for fluoride removal from aqueous solution. However, the nano-powder form of the adsorbent makes it difficult to be immobilized, separated and recycled in the practical defluoridation process. Therefore, the design of novel granular adsorption materials is needed to remove fluoride in actual wastewater.

As an alternative, powder adsorption materials can be immobilized into porous structured calcium–alginate beads as a particulate form. Alginate is a nontoxic, hydrophilic, and biocompatible natural polymer that is produced by brown algae, and can form an insoluble hydrogel in the presence of divalent and trivalent cations as a gelling agent through ionic interaction between the carboxylic acid group located on the polymer backbone and the chelating cations.[14] Entrapment using calcium–alginate beads is widely used in immobilization of various powdered materials to remove target pollutants from an aqueous solution because it is a simple and cost effective technique. Therefore, SA has been investigated in many researches for heavy metal removal, such as Pb^{2+},[15–17] Cu^{2+} (ref. 18 and 19) and Cd^{2+}.[20,21] Until now, calcium alginate had been used in immobilizing hydrous ferric oxide,[22] Fe–Zr binary mixed oxide[23] and Ce–Zr oxide[24] to remove fluoride in wastewater. However, the low adsorption affinity for the fluoride has limited their use in the wastewater treatment.

[a]School of Metallurgy and Environment, Central South University, Changsha 410083, China. E-mail: zhoukg63@163.com
[b]School of Municipal and Mapping Engineering, Hunan City University, Yiyang 413000, China

The present study aims at developing Mg–Al–La composite oxides doped calcium alginate beads for fluoride mitigation from wastewater. The beads were synthesized at ambient temperature. The surface and structural properties of the synthesized adsorbent was characterized by scanning electron microscopy (SEM), X-ray photoelectron spectroscopy (XPS) and Fourier transform infrared spectroscopy (FT-IR). Batch adsorption experiments were carried out to investigate the fluoride removal efficiency of the prepared beads. Various adsorption isotherms and kinetic models were fitted to understand the adsorption process.

2. Materials and methods

2.1 Materials

All chemicals used were of analytical grade. $MgCl_2 \cdot 6H_2O$, $AlCl_3 \cdot 6H_2O$, $LaCl_3 \cdot 6H_2O$ were purchased from Sinopharm Chemical Reagent Co., Ltd. (Shanghai, China). Deionized water was used in all experiments. Stock solution of fluoride was prepared by dissolving 2.21 g of sodium fluoride in 1 L deionized water. The target concentration of fluoride solution was prepared by serial dilution of 1000 mg L^{-1} fluoride solution.

2.2 Preparation of Mg–Al–La mixed oxide composite

Mg–Al–La was obtained by a conventional co-precipitation method. One solution (300 mL) contained $MgCl_2 \cdot 6H_2O$, $AlCl_3 \cdot 6H_2O$ and $LaCl_3 \cdot 6H_2O$. The concentration of metal cation was 1 mol L^{-1}, and the ratio of Mg : Al : La was 20 : 1 : 4. Another solution (300 mL) contained 2 M NaOH and 0.5 M Na_2CO_3, which was enough to precipitate the salt in the first solution. The two solutions were simultaneously added dropwise into 400 mL deionized water with vigorously stirring. The temperature was fixed at 60 °C, and the pH was maintained at 9–10. The resulting slurry was then aged at 60 °C for 24 h. The final precipitate was centrifuged several times with deionized water, till the superstratum water is free of Cl^-. The precipitate was dried at 80 °C for 24 h to obtain the Mg–Al–La power (100 mesh), and calcined Mg–Al–La power was obtained by calcining Mg–Al–La in a muffle furnace at 500 °C for 5 h. The sample obtained was marked as CMAL.

2.3 Preparation of Mg–Al–La loaded alginate bead

In order to prepare the Mg–Al–La loaded calcium alginate bead, 10.0 g of sodium alginate powder was dispersed in 500 mL deionized water. This was achieved by stirring at 150 rpm and keeping solution temperature at 80 °C for 1 h. Then, 40 g of CMAL was added into the viscous solution and further stirred for another 1 h. Thus Mg–Al–La loaded calcium alginate beads were obtained by dropwise adding the viscous solution (using a glass syringe) to 2% $CaCl_2$ solution with slow stirring. As a result, beads of approximately 2–3 mm in diameter were formed. The beads were allowed to keep in contact with $CaCl_2$ solution for 24 h. This process led to the formation of stable gel beads. Finally, all beads were washed several times with deionized water and dried in the vacuum drying chamber at 50 °C for 24 h. The sample obtained was marked as SA-CMAL.

2.4 Batch adsorption study

Batch adsorption experiments were conducted to test the performance of SA-CMAL beads as fluoride adsorbents. The influence of initial pH and co-existing anions, along with adsorption kinetics and adsorption isotherms were investigated. A known quantity of beads were mixed with a specific volume of known fluoride solution and agitated at constant temperature for different time intervals to determine equilibrium conditions. The filtrate was collected in polythene tubes and diluted before analysis. The concentration of remaining fluoride ions in the adsorption medium was determined by fluoride ion selective electrode. All the experiments were conducted in triplicates.

The effect of initial solution pH variation was studied by mixing 5 g L^{-1} of SA-CMAL beads with 100 mL of 40 mg L^{-1} fluoride solution in a polyethylene centrifuge. The initial pH values of the solution were then adjusted from 2 to 13 using 0.01 M HCl or NaOH solution. The centrifuge tubes containing the mixtures were fixed on a shaking table (operating at 150 rpm) at 303 K. After overnight mixing, the sample mixtures were filtrated through a 0.22 μm GE cellulose nylon membrane filter and the filtrate were analyzed by fluoride ion selective electrode. The initial concentrations C_0 and anion concentration C_e (mg L^{-1}) at time t, were determined and the fluoride uptake Q_e (mg g^{-1}) was calculated from the equation $Q_e = V(C_0 - C_e)/m$, where V is the volume of the solution in mL and m is the mass of the adsorbent (g).

The adsorption kinetic experiment of fluoride on SA-CMAL was carried out by mixing 5 g L^{-1} SA-CMAL with the initial fluoride concentration of 60 mg L^{-1} in 1 L beaker. The mixtures in bottles were then stirred at 150 rpm at 298 K, 303 K, and 308 K. The extent of adsorption was analyzed at different time intervals up to 97 h, the mixtures were immediately filtered through a 0.22 μm GE cellulose nylon membrane filter. Then, the concentration of fluoride in the filtrate was analyzed. Pseudo-first-order, pseudo-second-order kinetic models and intra-particle diffusion models[25] as expressed in eqn (1)–(3) were used to fit the adsorption experiment data, respectively:

Pseudo-first-order kinetic model:

$$\lg Q_e - Q_t = \lg Q_e - \frac{k_1}{2.303} t \quad (1)$$

Pseudo-second-order kinetic model:

$$\frac{t}{Q_t} = \frac{1}{k_2 Q_e^2} + \frac{t}{Q_e} \quad (2)$$

Intra-particle diffusion model: $Q_t = k_p t^{0.5} + C$ (3)

where Q_e and Q_t are the amount of fluoride adsorbed at equilibrium and at time t. k_1, k_2 and k_p are the rate constants of pseudo-first-order kinetic model, pseudo second order kinetic model and intra-particle diffusion model, respectively. C is the intercept of intra-particle diffusion model.

Fluoride sorption isotherms on the SA-CMAL beads were determined by mixing 5 g L^{-1} SA-CMAL beads with 100 mL of

a series of fluoride solutions (pH 6.0, 10–200 mg L^{-1} fluoride) in a polyethylene bottle. After overnight mixing, the samples were filtrated through a 0.22 μm GE cellulose nylon membrane filter. The concentration of fluoride in the filtrate was analyzed. Langmuir and Freundlich isotherm models[26] shown in eqn (4) and (5) were used for fluoride adsorption isotherms, respectively:

Langmuir isotherm model:

$$\frac{C_e}{Q_e} = \frac{1}{Q_0 b} + \frac{C_e}{Q_0} \quad (4)$$

Freundlich isotherm model:

$$\lg Q_e = \lg K_f + \frac{1}{n} \lg C_e \quad (5)$$

where C_e, Q_e, and Q_0 are the residual fluoride concentration at equilibrium, the fluoride concentration adsorbed on the sorbent at equilibrium, and the maximum fluoride concentration, respectively, and b, K_f, and n are the Langmuir constant, the Freundlich constant, and adsorption intensity, respectively.

The effects of co-existing anions on fluoride adsorption was evaluated by mixing 5 g L^{-1} SA-CMAL beads with 100 mL of fluoride solution (pH 6.0, 40 mg L^{-1} fluoride) containing a certain concentrations of co-existing anions (including PO_4^{3-}, NO_3^-, CO_3^{2-} and SO_4^{2-}) in a polyethylene bottle. Solution without co-existing anions was used as blank test. After overnight equilibration, the mixture was filtrated through a 0.22 μm GE cellulose nylon membrane filter, and then analyzed for fluoride concentration.

2.5 Analytical measurements

The FTIR spectra of all the sample materials were recorded at room temperature at a resolution of 4 cm^{-1} with 64 scans using Shimadzu IR Prestige-21 FTIR instrument. SEM images of the samples were obtained in a JSM 6390 LV apparatus. The optical microscopic image was taken using Leica EZ 4D optical microscope. XPS measurements (ESCALAB250, Thermo Fisher Corporation, USA) of absorbent before and after adsorption were carried out to obtain the elements binding energies of SA-CMAL and SA-CMAL-F. Concentrations of fluoride in the solution, before and after adsorption, were determined using ion selective electrode (Orion 720A+ Ion analyzer).

3. Results and discussion

3.1 Effects of initial pH on fluoride adsorption

The pH is an important factor that may affect the adsorption process since it can change the surface charges of adsorbent.[27] The effect of initial pH values on sorption of fluoride to SA-CMAL is shown in Fig. 1.

The results show that, the initial pH values had negligible effect on fluoride adsorption in the pH range of 2–10, indicating that the SA-CMAL exhibited good fluoride removal property in a wide pH range. The acid pH condition was more beneficial for the fluoride removal by the SA-CMAL adsorbent. The fluoride

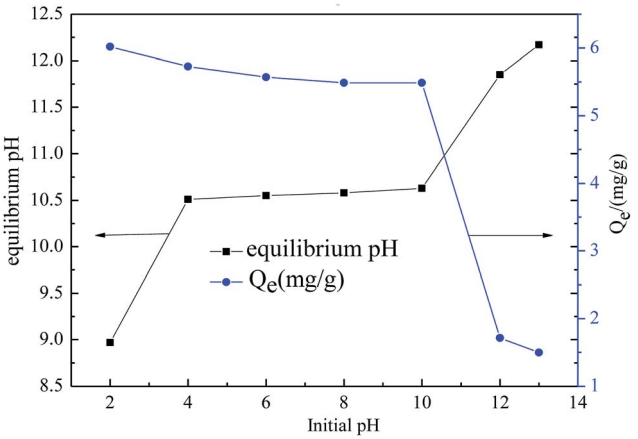

Fig. 1 Effect of initial pH on fluoride adsorption *via* SA-CMAL.

adsorption amount was above 5 mg g^{-1} at pH 2–10 condition and decreased sharply to 1.7 mg g^{-1} when the initial pH was up to 12. The higher adsorption fluoride capacity at acid pH condition might be ascribed to the consumption of hydroxyl ions in water by hydrogen ions, which promotes the exchange of F^- and M − OH groups. On the other hand, the lower fluoride removal rate at alkaline pH condition might be attributed to the competition between fluoride and hydroxyl ions.[28]

The final pH values after adsorption were also measured and shown in Fig. 1. It can be seen that the equilibrium pH values increased with the initial pH values. The increase in pH values after adsorption was associated with the protonation of hydroxyl groups on the material surface. In addition, the ligand exchange between OH^- and fluoride might release the OH^- that would increase the equilibrium pH values of the solution.

3.2 Adsorption isotherms

The Langmuir and Freundlich isotherms are fundamental models to describe and understand adsorption process. The Langmuir isotherm model is often applied for monolayer adsorption onto a surface containing certain number of identical sites. The Freundlich isotherm model is valid for multilayer adsorption onto a heterogeneous surface.[29] The adsorption data of isotherms are presented in Fig. 2 at different temperatures. The parameters for the fitting of linear Langmuir isotherm (eqn (4)) and the linear Freundlich isotherm(eqn (5)) are shown in Table 1 (Fig. 3).

As shown in Fig. 2 and Table 1, comparing with the correlation coefficients (R^2) of Langmuir and Freundlich, the adsorption isotherms with SA-CMAL particles can be well described by the Freundlich isotherm, which suggested that the adsorption occurred on the heterogeneous surfaces of the adsorbent. In addition, the Langmuir constant b has a positive value and all values of the Freundlich constant n were between 1 and 10, confirming that the adsorption was favorable. Table 2 shows the fluoride adsorption capacity of the SA-CMAL compared with other adsorbents that have been reported. It is worth noting that the fluoride adsorption capacity of SA-CMAL

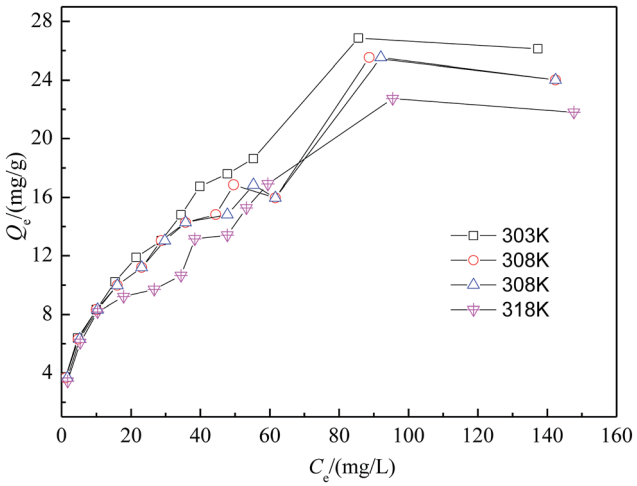

Fig. 2 Adsorption isotherms of fluoride on SA-CMAL at 303 K, 308 K, 313 K and 318 K.

is much higher than those of other adsorbents, indicating a potential application for fluoride removal.

3.3 Thermodynamic investigations

The effect of temperature may have a significant influence on the sorption process. Hence the sorption of SA-CMAL was monitored at four different temperatures 303 K, 308 K, 313 K and 318 K under the optimized condition, and thermodynamic parameters *viz.* standard free energy change (ΔG^0), standard enthalpy change (ΔH^0) and standard entropy change (ΔS^0) were calculated from eqn (6) and (7).[35]

$$\Delta G^0 = -RT \ln K_d \quad (6)$$

$$\ln K_d = \frac{\Delta S^0}{R} - \frac{\Delta H^0}{RT} \quad (7)$$

where R is the universal gas constant (8.314 J (mol K)$^{-1}$), and T is the temperature in Kelvin. The thermodynamic equilibrium constants (K_d) of the fluoride adsorption on SA-CMAL were calculated from the intercept of the plots of $\ln(Q_e/C_e)$ *versus* Q_e. The resulted are presented in Table 3.

Table 2 Comparison between various adsorbents used for fluoride removal

Name of sorbent	Adsorption capacity (mg g^{-1})	Reference
Granular ferric hydroxide	9.00	30
La(III)-loaded bentonite/chitosan beads	2.87	31
Granular acid-treated bentonite	0.278	32
Granular zirconium-iron oxide	9.80	33
FZCA(Fe/Zr)–alginate	0.981	23
n-HApAlg composite	0.123	34
SA-CMAL	30.98	Present study

Table 1 Parameters of Langmuir and Freundlich adsorption isotherm models for fluoride adsorbed by SA-CMAL at different temperatures

		T (K)			
Isotherm	Parameters	303	308	313	318
Langmuir	b (L mg^{-1})	0.03520	0.03741	0.03367	0.03255
	Q_0 (mg g^{-1})	30.96	27.70	27.32	25.91
	R^2	0.9276	0.9151	0.8951	0.9086
Freundlich	K_f (mg g^{-1}) (L mg^{-1})$^{1/n}$	3.275	3.274	2.685	2.775
	$1/n$	0.4327	0.4107	0.4290	0.4233
	R^2	0.9837	0.9777	0.9743	0.9653

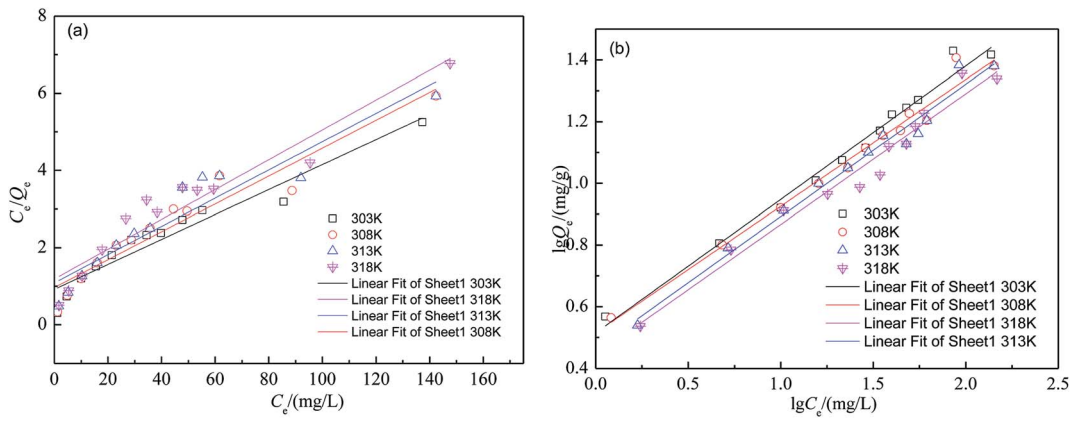

Fig. 3 Linearization of the Langmuir isotherm (a) and the Freundlich isotherm (b) for fluoride adsorption on SA-CMAL.

Table 3 Thermodynamic parameters of fluoride sorption on SA-CMAL

	Thermodynamic parameters		
Temperature (K)	ΔG^0 (kJ mol^{-1})	ΔH^0 (kJ mol^{-1})	ΔS^0 (J (mol K)$^{-1}$)
303	−0.7975	−10.89	−0.03327
308	−0.6886		
313	−0.4471		
318	−0.3234		

All the thermodynamic parameters were negative values. The negative values of ΔG^0 indicated the spontaneity of the sorption reaction. The negative values of ΔH^0 indicated the exothermic nature of the sorption reaction. The negative value of ΔS^0 indicated a decrease in the order of the sorption of fluoride on SA-CMAL.

3.4 Adsorption kinetics

Contact time is one of the important parameters influencing the efficiency of the adsorption process. The kinetic study was conducted for fluoride adsorption onto SA-CMAL at adsorbent dose of 3 g L^{-1} and initial fluoride concentration of 60 mg L^{-1} at temperatures 298 K, 303 K and 308 K, respectively. The experiments were conducted by varying time between 0.33 h and 97 h. It is evident from Fig. 4 that uptake increased with time and gradually reached to the maximum. The uptake of fluoride was fast within 48 h, after which it slowed down and the equilibrium approached. This might be due to the reduction of driving force after long operation period. Initially the sorbent sites were vacant, hence uptake was increasing with time. Then the sites were filled with fluoride and ultimately saturated.

In order to understand the mechanism of fluoride sorption on SA-CMAL, the pseudo-first-order kinetic, pseudo-second-order kinetic, and intra-particle diffusion were applied to simulate the adsorption data. The plots are given in Fig. 5. And the calculated kinetic parameters together with the regression coefficients (R^2) are listed in Table 4. It can be observed that the R^2 of pseudo-second-order model were much higher than those of the pseudo-first-order model at different temperature. Moreover, the experimental adsorption capacity ($Q_{e,exp}$) values matched well with the theoretical adsorption capacity ($Q_{e,cal}$) values calculated from the pseudo-second-order model compared with that calculated from the pseudo-first-order model. The results indicated that the fluoride adsorption process can be well described by the pseudo-second-order model and the adsorption process might be chemisorption.[36]

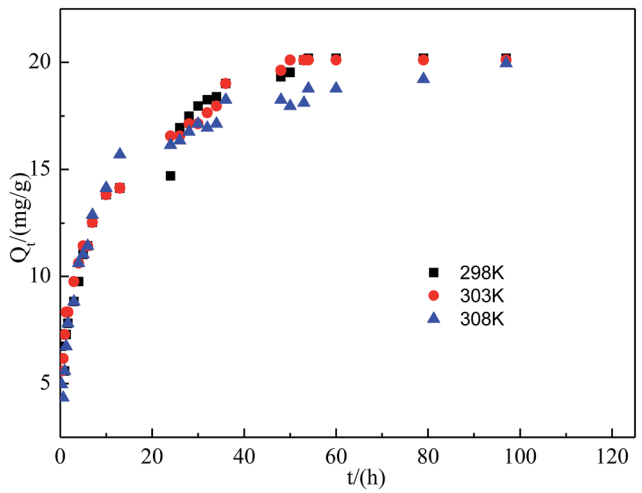

Fig. 4 Adsorption kinetics of fluoride on SA-CMAL at different temperature.

The intra-particle diffusion model was applied to further investigate the rate limiting step of the adsorption process. In general, the process of fluoride adsorption follows three consecutive steps:[37] (1) transport of fluoride from boundary film to the exterior surface of adsorbent (film diffusion); (2) transfer of fluoride from the surface to the pores of adsorbent (intra-particle diffusion); (3) adsorption of fluoride on the interior surface of adsorbent (equilibrium stage).

The plot of Q_t *vs.* $t^{0.5}$ at different temperature is shown in Fig. 5c and the constants calculated from the plot are listed in Table 4. The results show that the curves presented multi-linearity, which indicated that the adsorption processes were not only controlled by intra-particle diffusion. The linear portions of the curves did not pass through the zero point indicating that mechanism of fluoride removal by SA-CMAL is complex and both the surface adsorption and intra-particle diffusion contributed to the rate determining step.

3.5 Effect of co-existing anions on fluoride uptake

Phosphate, carbonate, sulfate and nitrate are typically present in fluoride-contaminated water and may compete with fluoride for active adsorption sites. The effect of coexisting anions was investigated by adding the coexisting anions (concentration ranging from 0.01 to 0.1 mol L^{-1}) into the mixture of SA-CMAL (5 g L^{-1}) and fluoride (40 mg L^{-1}). The effects of co-existing anions on fluoride uptake are present in Fig. 6.

As shown in Fig. 6, both SO_4^{2-} and NO_3^- had small impact on the fluoride adsorption capacity, which were dropped by 19.5% and 14.6% respectively at the concentration of 0.1 mol L^{-1}. However, significant decreases of fluoride adsorption capacity occurred with the co-existing anions of CO_3^{2-} or PO_4^{3-}. The reduction in fluoride adsorption capacity by the SA-CMAL in the presence PO_4^{3-}, SO_4^{2-}, CO_3^{2-} and NO_3^- could be possibly attributed to the competition of active sorption sites on the adsorbent. The ratio of charge towards radius (z/r) of the anions was closely correlated with their affinity to the adsorbent. The z/r values of the anions are in the order of PO_4^{3-} (3/3.40) > CO_3^{2-} (2/1.64) > SO_4^{2-} (2/2.44) > NO_3^- (1/1.65).[38]

3.6 Characterization of SA-CMAL

3.6.1 Surface morphology analysis. The digital photos of dry SA-CMAL particles are present in Fig. 7a. The SEM images of SA-CMAL before and after fluoride adsorption are shown in Fig. 7. The surface of the fresh SA-CMAL was compact (Fig. 7b).

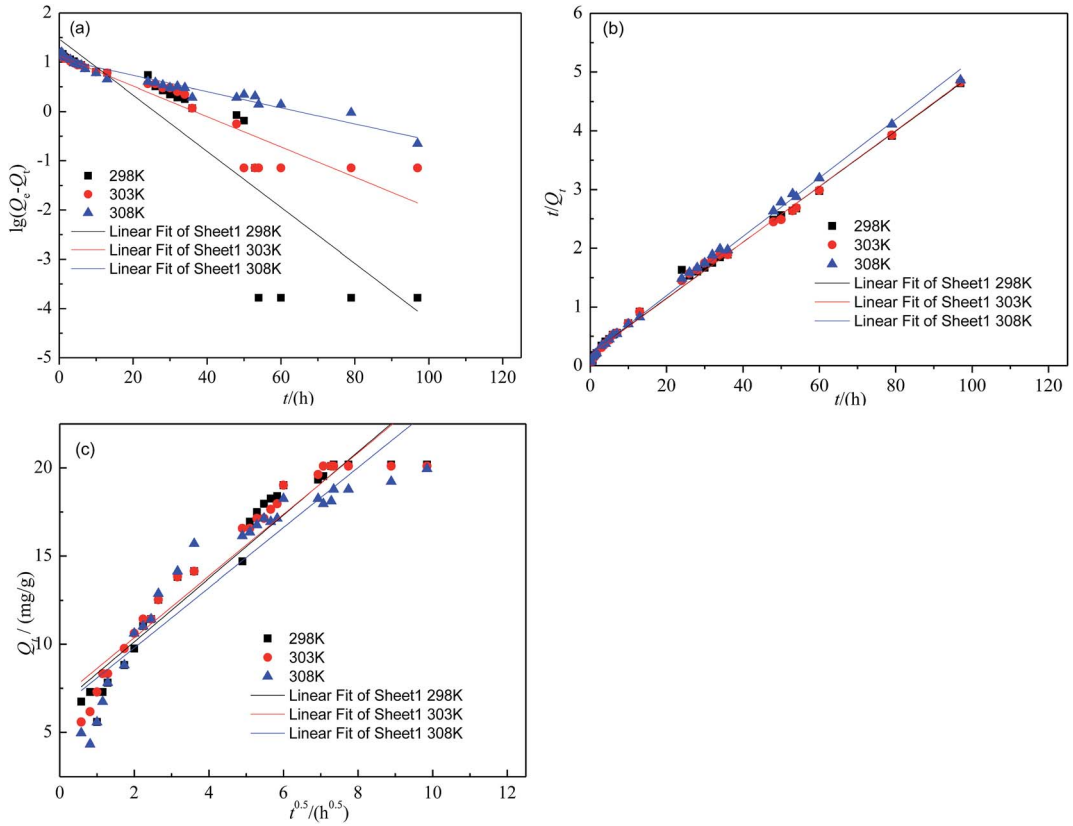

Fig. 5 Linearization of pseudo-first-order kinetic model (a), pseudo-second-order kinetic model (b) and intra-particle diffusion (c) for fluoride adsorption on SA-CMAL at different temperature.

After fluoride adsorption, it became rough and loose (Fig. 7c), and some tiny interspaces were present.

3.6.2 FTIR analysis. FTIR spectra analysis was performed to show the functional groups on the materials. The FTIR spectra of SA-CMAL before and after adsorption are presented in Fig. 8.

Table 4 Parameters of pseudo-first-order kinetic model, pseudo-second-order kinetic model and intra-particle diffusion model for fluoride adsorbed by SA-CMAL at different temperatures

	T (K)		
Kinetic model	303	308	313
$Q_{e,exp}$	20.17	20.10	19.95
Pseudo-first-order			
$Q_{e,cal}$ (mg g^{-1})	29.56	13.49	11.51
K_1 (min^{-1})	0.05694	0.03079	0.01639
R^2	0.7816	0.8685	0.9431
Pseudo-second-order			
$Q_{e,cal}$ (mg g^{-1})	21.07	20.95	19.98
K_2 (g (mg h)$^{-1}$)	0.01125	0.01210	0.01286
h (mg (g h)$^{-1}$)	4.993	5.308	5.133
R^2	0.9945	0.9953	0.9968
Intraparticle diffusion			
K_{ip} (mg (g h)$^{-0.5}$)	1.795	1.748	1.703
C	6.555	6.881	6.392
R^2	0.9132	0.9196	0.8692

The broad peak at 3460 cm^{-1} was assigned to the stretching models of O–H bands, and the peaks at 1624 cm^{-1} and 1508 cm^{-1} corresponded to –COO– anti-symmetric stretching vibration and symmetric stretching vibration, respectively. The peak at 1059 cm^{-1} indicated the presence of C–O group. The comparison of FT-IR spectra before and after fluoride adsorption (Fig. 8a and b) shows that the peaks at 3460 cm^{-1}, 1624

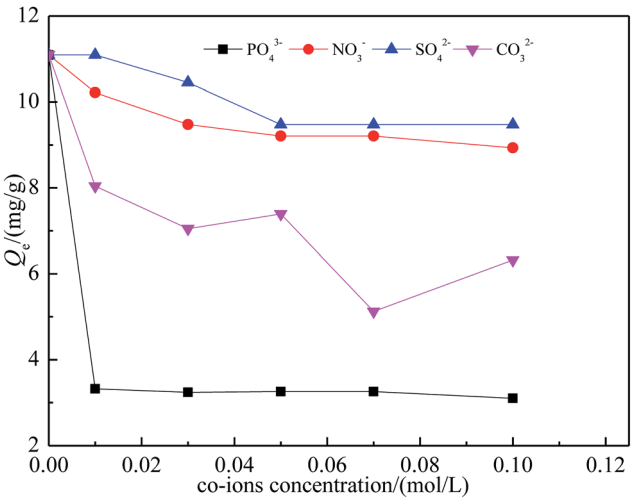

Fig. 6 Effect of co-ions on fluoride adsorption by SA-CMAL.

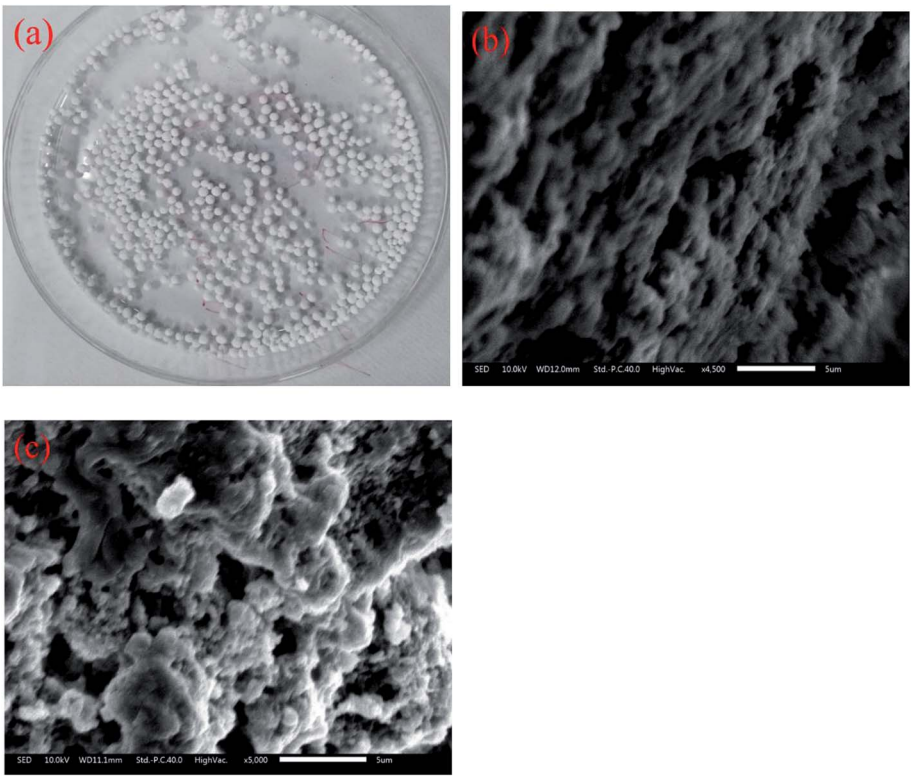

Fig. 7 SEM of SA-CMAL dry beads (a), before (b) and after (c) adsorbed by fluoride.

cm^{-1} and 1508 cm^{-1} shifted to 3447 cm^{-1}, 1629 cm^{-1} and 1509 cm^{-1}, respectively. The shifts indicated that hydroxyl and carboxyl groups participated in the adsorption process, since the removal amount of fluoride was directly related to the presence of these sites on the adsorbent. In addition, the bands at 463 cm^{-1} and 410 cm^{-1} shifted to 450 cm^{-1} and 428 cm^{-1}, respectively, and a new peak appeared at 562 cm^{-1} after adsorption, indicating that the interaction occurred between the metal ions and the fluoride in the adsorption process.

3.6.3 XPS analysis. To further understand the elemental information of the SA-CMAL particles and the interaction between adsorbent and fluoride, the XPS spectra of SA-CMAL particles before and after fluoride adsorption are shown in Fig. 9. The wide scan XPS spectra showed that the main elements in the shell of the adsorbent were C, O, Mg, Al, La and Ca. After adsorption, a new F 1s peak was found at 684.1 eV, indicating the existence of fluoride on the adsorbent surface. These results confirmed that the adsorbent was effective for fluoride removal. The high fluoride removal efficiency can be attributed to isomorphic substitution between F^- and OH^-.

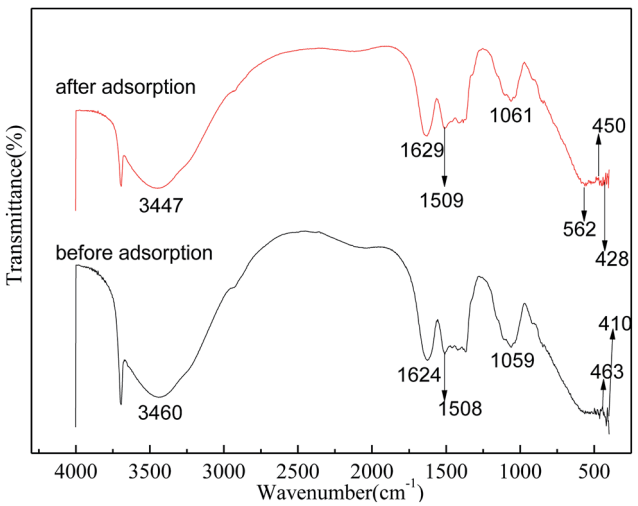

Fig. 8 FTIR of before and after fluoride adsorption on SA-CMAL.

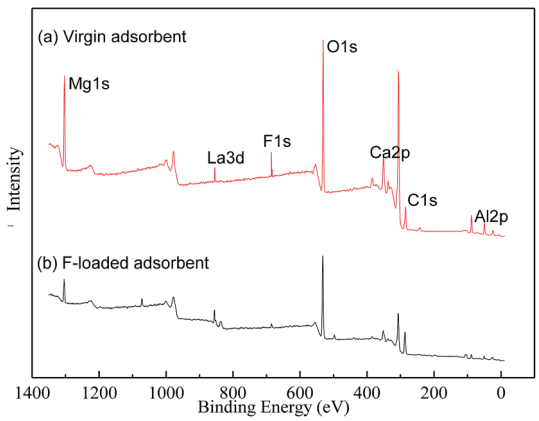

Fig. 9 XPS wide scan spectra of the adsorbents: (a) virgin adsorbent; (b) F-loaded adsorbent.

4. Conclusion

In the present work, a novel SA-CMAL adsorbent was successfully designed for fluoride removal from aqueous solutions *via* entrapment of the Mg–Al–La composite oxides powder into alginate beads. The result indicated that the beads could remove fluoride effectively within a wide pH ranging from 2 to 10, indicating that there was no requirement to adjust the pH in treatment of industry wastewater. The presence of SO_4^{2-} and NO_3^- had slight effects on the fluoride removal, while CO_3^{2-} and PO_4^{3-} decreased the fluoride adsorption efficiency. Under the optimal condition: pH of 6.0, contact time of 24 h, 5 g L^{-1} of the dose, and the temperature of 303 K, the maximum uptake capacity of SA-CMAL is 30.96 mg g^{-1}. The equilibrium data could be better fitted by the Freundlich model than the Langmuir model. The adsorption kinetic data can be well described by pseudo-second-order model for fluoride. The value of ΔH^0 and ΔG^0 indicate that the process of fluoride adsorption is spontaneous and exothermic. From the analysis of FTIR, XPS, kinetic and thermodynamic parameters, it can be presumed that the physical adsorption and chemical adsorption corporately controlled adsorption stage.

Acknowledgements

This work was supported by the National Natural Science Foundation of China (No. 51174328).

References

1 M. Mohapatra, D. Hariprasad, L. Mohapatra, S. Anand and B. K. Mishra, Mg-doped nano ferrihydrite-A new adsorbent for fluoride removal from aqueous solutions, *Appl. Surf. Sci.*, 2012, **258**, 4228–4236.

2 L. M. Camacho, A. Torres, D. Saha and S. Deng, Adsorption equilibrium and kinetics of fluoride on sol–gel-derived activated alumina adsorbents, *J. Colloid Interface Sci.*, 2010, **349**, 307–313.

3 C. Liu and J. C. Liu, Coupled precipitation-ultrafiltration for treatment of high fluoride-content wastewater, *J. Taiwan Inst. Chem. Eng.*, 2016, **58**, 259–263.

4 K. Jiang, K. Zhou, Y. Yang and H. Du, A pilot-scale study of cryolite precipitation from high fluoride-containing wastewater in a reaction-separation integrated reactor, *J. Environ. Sci.*, 2013, **25**, 1331.

5 Y. Xiao, T. Chen, Y. Hu, D. Wang, Y. Han, Y. Lin and X. Wang, Advanced treatment of semiconductor wastewater by combined MBR–RO technology, *Desalination*, 2014, **336**, 168–178.

6 K. Govindan, M. Raja, S. Uma Maheshwari, M. Noel and Y. Oren, Comparison and understanding of fluoride removal mechanism in Ca^{2+}, Mg^{2+} and Al^{3+} ion assisted electrocoagulation process using Fe and Al electrodes, *J. Environ. Chem. Eng.*, 2015, **3**, 1784–1793.

7 V. Khatibikamal, A. Torabian, F. Janpoor and G. Hoshyaripour, Fluoride removal from industrial wastewater using electrocoagulation and its adsorption kinetics, *J. Hazard. Mater.*, 2010, **179**, 276–280.

8 L. Chai, Y. Wang, N. Zhao, W. Yang and X. You, Sulfate-doped Fe_3O_4/Al_2O_3 nanoparticles as a novel adsorbent for fluoride removal from drinking water, *Water Res.*, 2013, **47**, 4040–4049.

9 A. Ben Nasr, K. Walha, C. Charcosset and R. Ben Amar, Removal of fluoride ions using cuttlefish bones, *J. Fluorine Chem.*, 2011, **132**, 57–62.

10 X. Xu, Q. Li, H. Cui, J. Pang, L. Sun, H. An and J. Zhai, Adsorption of fluoride from aqueous solution on magnesia-loaded fly ash cenospheres, *Desalination*, 2011, **272**, 233–239.

11 H. Paudyal, B. Pangeni, K. Inoue, H. Kawakita, K. Ohto and S. Alam, Adsorptive removal of fluoride from aqueous medium using a fixed bed column packed with Zr(IV) loaded dried orange juice residue, *Bioresour. Technol.*, 2013, **146**, 713–720.

12 A. Ghosh, S. Chakrabarti, K. Biswas and U. C. Ghosh, Agglomerated nanoparticles of hydrous Ce(IV) + Zr(IV) mixed oxide: Preparation, characterization and physicochemical aspects on fluoride adsorption, *Appl. Surf. Sci.*, 2014, **307**, 665–676.

13 A. Dhillon, M. Nair, S. K. Bhargava and D. Kumar, Excellent fluoride decontamination and antibacterial efficacy of Fe–Ca–Zr hybrid metal oxide nanomaterial, *J. Colloid Interface Sci.*, 2015, **457**, 289–297.

14 S. N. Gasmi, C. Rihouey, L. Picton and C. D. Le, Hydrolysis of pullulan by entrapped pullulanase in Ca/alginate beads., *Biopolymers*, 2014, **101**, 938.

15 Z. Wang, Y. Huang, M. Wang, G. Wu, T. Geng, Y. Zhao and A. Wu, Macroporous calcium alginate aerogel as sorbent for Pb^{2+} removal from water media, *J. Environ. Chem. Eng.*, 2016, **4**, 3185–3192.

16 L. Jiao, P. S. Qi, Y. Z. Liu and B. Wang, Fe_3O_4 and TiO_2 Embedded Sodium Alginate Beads of Composite Adsorbent for Pb(II) Removal, *Adv. Mater. Res.*, 2014, **900**, 160–164.

17 R. Verma, A. Asthana, A. K. Singh, S. Prasad and M. A. B. H. Susan, Novel glycine-functionalized magnetic nanoparticles entrapped calcium alginate beads for effective removal of lead, *Microchem. J.*, 2016, **130**, 168–178.

18 N. Jiang, Y. Xu, Y. Dai, W. Luo and L. Dai, Polyaniline nanofibers assembled on alginate microsphere for Cu^{2+} and Pb^{2+} uptake, *J. Hazard. Mater.*, 2012, **215–216**, 17–24.

19 Y. Lai, M. Thirumavalavan and J. Lee, Effective adsorption of heavy metal ions (Cu^{2+}, Pb^{2+}, Zn^{2+}) from aqueous solution by immobilization of adsorbents on Ca-alginate beads, *Toxicol. Environ. Chem.*, 2010, **92**, 697–705.

20 F. Wang, X. Lu and X. Y. Li, Selective removals of heavy metals (Pb^{2+}, Cu^{2+}, and Cd^{2+}) from wastewater by gelation with alginate for effective metal recovery, *J. Hazard. Mater.*, 2016, **308**, 75–83.

21 S. K. Papageorgiou, F. K. Katsaros, E. P. Kouvelos and N. K. Kanellopoulos, Prediction of binary adsorption isotherms of Cu^{2+}, Cd^{2+} and Pb^{2+} on calcium alginate beads from single adsorption data., *J. Hazard. Mater.*, 2009, **162**, 1347.

22 M. G. Sujana, A. Mishra and B. C. Acharya, Hydrous ferric oxide doped alginate beads for fluoride removal: Adsorption kinetics and equilibrium studies, *Appl. Surf. Sci.*, 2013, **270**, 767–776.

23 S. K. Swain, T. Patnaik, P. C. Patnaik, U. Jha and R. K. Dey, Development of new alginate entrapped Fe(III)–Zr(IV) binary mixed oxide for removal of fluoride from water bodies, *Chem. Eng. J.*, 2013, **215–216**, 763–771.

24 L. Chen, K. Zhang, J. He, X. G. Cai, W. Xu and J. H. Liu, Performance and mechanism of hierarchically porous Ce–Zr oxide nanospheres encapsulated calcium alginate beads for fluoride removal from water, *RSC Adv.*, 2016, **6**, 36296–36306.

25 Y. Cao, G. Li and X. Li, Graphene/layered double hydroxide nanocomposite: Properties, synthesis, and applications, *Chem. Eng. J.*, 2016, **292**, 207–223.

26 Y. Wang, F. Li, S. Dong, X. Liu and M. Li, A facile approach for synthesizing Fe-based layered double hydroxides with high purity and its exfoliation., *J. Colloid Interface Sci.*, 2016, **467**, 28.

27 T. Zhu, T. Zhu, J. Gao, L. Zhang and W. Zhang, Enhanced adsorption of fluoride by cerium immobilized cross-linked chitosan composite, *J. Fluorine Chem.*, 2017, **194**, 80–88.

28 D. Tang and G. Zhang, Efficient removal of fluoride by hierarchical Ce–Fe bimetal oxides adsorbent: Thermodynamics, kinetics and mechanism, *Chem. Eng. J.*, 2016, **283**, 721–729.

29 Y. Zhang and Y. Jia, Fluoride adsorption onto amorphous aluminum hydroxide: Roles of the surface acetate anions, *J. Colloid Interface Sci.*, 2016, **483**, 295–306.

30 Y. Tang, X. Guan, J. Wang, N. Gao, M. R. McPhail and C. C. Chusuei, Fluoride adsorption onto granular ferric hydroxide: Effects of ionic strength, pH, surface loading, and major co-existing anions, *J. Hazard. Mater.*, 2009, **171**, 774–779.

31 Y. Zhang, Y. Xu, H. Cui, B. Liu, X. Gao, D. Wang and P. Liang, La(III)-loaded bentonite/chitosan beads for defluoridation from aqueous solution, *J. Rare Earths*, 2014, **32**, 458–466.

32 Y. Ma, F. Shi, X. Zheng, J. Ma and C. Gao, Removal of fluoride from aqueous solution using granular acid-treated bentonite (GHB): Batch and column studies, *J. Hazard. Mater.*, 2011, **185**, 1073–1080.

33 X. Dou, Y. Zhang, H. Wang, T. Wang and Y. Wang, Performance of granular zirconium–iron oxide in the removal of fluoride from drinking water, *Water Res.*, 2011, **45**, 3571–3578.

34 K. Pandi and N. Viswanathan, Synthesis of alginate bioencapsulated nano-hydroxyapatite composite for selective fluoride sorption, *Carbohydr. Polym.*, 2014, **112**, 662–667.

35 L. Yan, K. Yang, R. Shan, T. Yan, J. Wei, S. Yu, H. Yu and B. Du, Kinetic, isotherm and thermodynamic investigations of phosphate adsorption onto core–shell Fe_3O_4@LDHs composites with easy magnetic separation assistance, *J. Colloid Interface Sci.*, 2015, **448**, 508–516.

36 J. Cai, Y. Zhang, B. Pan, W. Zhang, L. Lv and Q. Zhang, Efficient defluoridation of water using reusable nanocrystalline layered double hydroxides impregnated polystyrene anion exchanger, *Water Res.*, 2016, **102**, 109–116.

37 E. Christina and P. Viswanathan, Development of a novel nano-biosorbent for the removal of fluoride from water, *Chin. J. Chem. Eng.*, 2015, **23**, 924–933.

38 L. Lv, J. He, M. Wei, D. Evans and X. Duan, Factors influencing the removal of fluoride from aqueous solution by calcined Mg–Al–CO_3 layered double hydroxides, *J. Hazard. Mater.*, 2006, **133**, 119–128.